Journal of Biomechanics 83 (2019) 260–272

Contents lists available at ScienceDirect

Journal of Biomechanics

journal homepage: www.elsevier.com/locate/jbiomech
www.JBiomech.com

Foot arch deformation and plantar fascia loading during running with rearfoot strike and forefoot strike: A dynamic finite element analysis

Tony Lin-Wei Chen [a], Duo Wai-Chi Wong [a,b], Yan Wang [a,b], Jin Lin [c], Ming Zhang [b,a,*]

[a] Department of Biomedical Engineering, Faculty of Engineering, The Hong Kong Polytechnic University, Hong Kong Special Administrative Region, China
[b] The Hong Kong Polytechnic University Shenzhen Research Institute, Shenzhen, China
[c] Product Development – R&D Life Nurturing Products, Infinitus (China) Company Ltd., Guangzhou, China

ARTICLE INFO

Article history:
Accepted 3 December 2018

Keywords:
Plantar fascia
Foot strike patterns
Finite element model

ABSTRACT

Forefoot strike becomes popular among runners because it facilitates better impact attenuation. However, forefoot strike may overload the plantar fascia and impose risk of plantar fasciitis. This study aimed to examine and compare the foot arch deformation and plantar fascia tension between different foot strike techniques in running using a computational modelling approach. A three-dimensional finite element foot model was reconstructed from the MRI of a healthy runner. The foot model included twenty bones, bulk soft tissue, ligaments, tendons, and plantar fascia. The time-series data of segmental kinematics, foot muscle force, and ankle joint reaction force were derived from a musculoskeletal model of the same participant based on the motion capture analysis and input as the boundary conditions for the finite element analysis. Rearfoot strike and forefoot strike running were simulated using a dynamic explicit solver. The results showed that, compared to rearfoot strike, forefoot strike reduced the foot arch height by 9.12% and increased the medial longitudinal arch angle by 2.06%. Forefoot strike also increased the plantar connective tissues stress by 18.28–200.11% and increased the plantar fascia tensile force by 18.71–109.10%. Although it is currently difficult to estimate the threshold value of stress or force that results in injury, forefoot strike runners appeared to be more vulnerable to plantar fasciitis.

1. Introduction

Plantar fasciitis was one of the most common lower limb injuries (van Gent et al., 2007). In the United States, more than two million individuals were diagnosed with plantar fasciitis on an annual basis, which was about 15% of all adult foot complaints (Roxas, 2005). Runners represented the most prevalent and vulnerable group to plantar fasciitis (Taunton et al., 2002). Though the pathologies of plantar fasciitis are not completely understood, repeated overload on the plantar fascia is considered as the primary biomechanical cause of the problem (Wearing et al., 2006).

Running style affected the mode of impact attenuation and force transmission that could be associated with the risks of injury (Daoud et al., 2012). To better attenuate impact shock, an increasing number of runners attempted to adopt a softer landing skill by modifying foot strike pattern (Altman and Davis, 2012). In spite of the benefits in reducing loading rate of the vertical ground reaction force (GRF) and knee joint force (Almeida et al., 2015; Knorz et al., 2017), forefoot strike (FFS) may impose threats to the foot arch and plantar connective tissues (Paquette et al., 2013; Perkins et al., 2014) compared to rearfoot strike (RFS). In FFS running, vertical GRF was applied anteriorly to the ankle center at touchdown. A larger Achilles tension was generated to maintain heel-lift and counteract ankle dorsiflexion caused by the GRF (Landreneau et al., 2014; Yong et al., 2014). Together with the body weight acting on the ankle, a three-point-bending loading mode was formed in the foot-and-ankle that compressed the longitudinal foot arch and overloaded the plantar connective tissues (Lieberman, 2012; Perl et al., 2012). Clinical studies have speculated the risks of plantar fasciitis involved in foot strike pattern modification (Daoud et al., 2012; Lieberman et al., 2010), in spite of that existing evidence is largely anecdotal.

Information of loading on the plantar connective tissues during running is essential to understand the relationship between foot strike patterns and plantar fasciitis. While in-vivo measurement of the plantar fascia force is usually difficult, computational modeling techniques can cater to the methodological needs. However, outcomes of existing simulation studies were inconclusive possibly due to some limitations inherent in the modeling details. Musculoskeletal model was robust to estimate the muscle forces that

* Corresponding author at: The Hong Kong Polytechnic University Shenzhen Research Institute, Shenzhen, China.
E-mail address: ming.zhang@polyu.edu.hk (M. Zhang).

https://doi.org/10.1016/j.jbiomech.2018.12.007
0021-9290/

replicated human motion, but the assumption of using rigid bodies would hinder the constitution of soft tissues, such as the muscular and ligamental stabilizers of the foot arch (Bruening et al., 2012). Finite Element (FE) model could predict segmental displacement and material deformation. Nevertheless, some existing studies implemented implicit solvers that ignored the large inertial moment of the bony structures generated in running (Behforootan et al., 2017). The load and compression on the soft tissue were heavily dependent on the momentum developed in transient and would be better predicted by an explicit solver (Chen and Lee, 2015). To increase the simulation accuracy, we presented a dynamic FE analysis with running gait characteristics. The innovation of this study also laid in using a relative accuracy dynamic model in addressing the biomechanics of foot strike patterns.

Therefore, the aims of this study were to (1) establish an FE foot model for dynamic simulation of running; (2) simulate RFS and FFS running; (3) compare the foot arch deformation and loading on

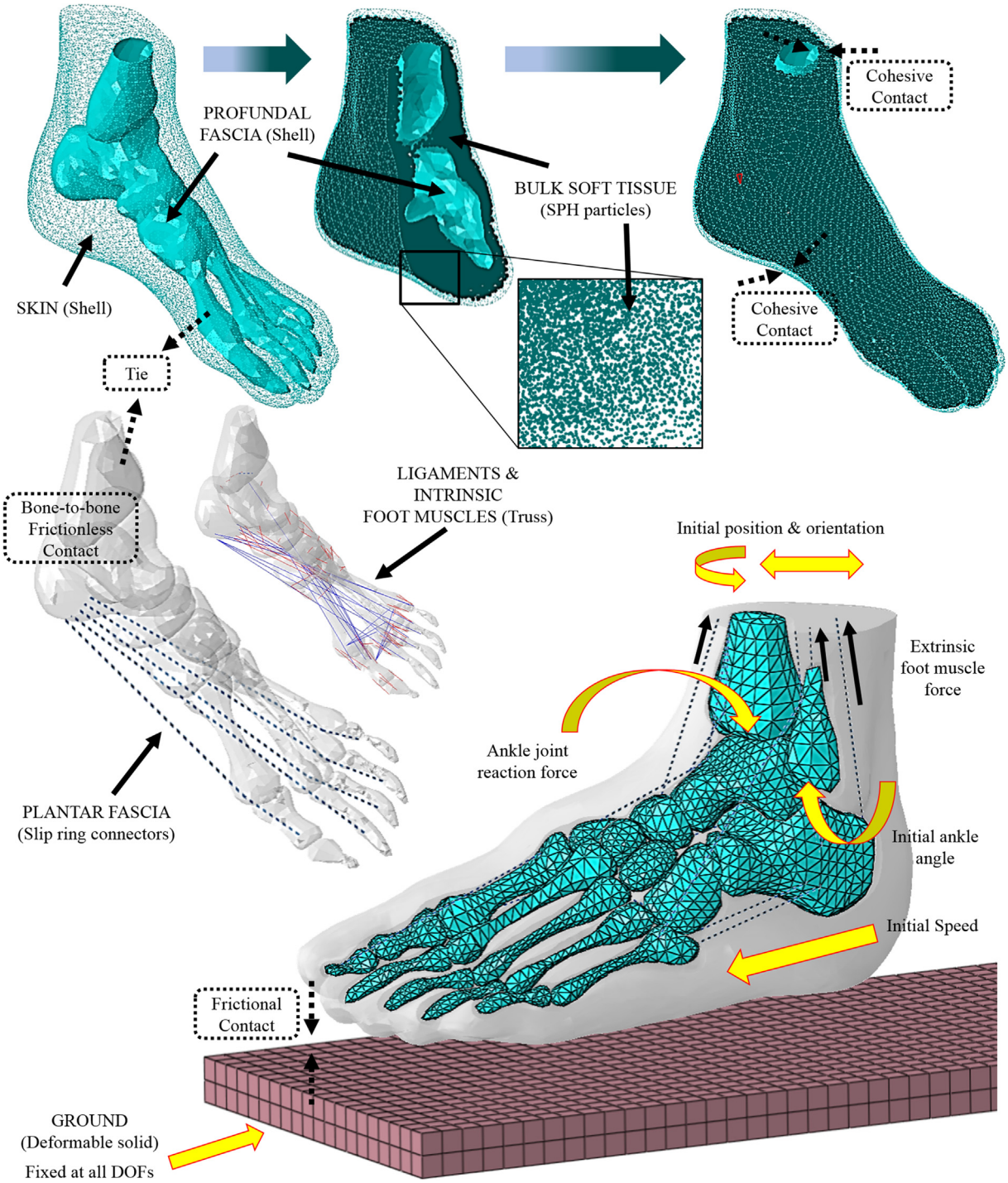

Fig. 1. Overview of FE foot model setup and boundary conditions. The bulk soft tissue was modeled as SPH particle elements and encapsulated in a shell unit with a interior profundal fascia layer and exterior skin layer. The internal layer of the shell was tied to the skeletal structures. The plantar foot was connected by ligaments (truss unit), intrinsic foot muscles (truss unit), and the plantar fascia (slip ring connector). The ground plate was fully fixed and the foot model was placed at an initial position/orientation with an initial ankle joint angulation. The three-dimensional ankle joint reaction force, extrinsic foot muscle force, and initial transitional velocity were applied to the model to drive the simulation. SPH: smoothed-particle hydrodynamics.

Table 1
Element type and material property assigned for the foot model components.

	Element	Material property	Density	Poisson's ratio	Mesh count	Reference
Skin	linear triangular shell (S3R)	Hyper-elastic (first-order Ogden model, μ = 0.122 kPa, α = 18) Thickness: 2.0 mm	950 kg/m^3	N/A	4,807	Pailler-Mattei et al., 2008
Bulk soft tissue	SPH particle (PC3D)	linearly elastic (Young's modulus: 800 kPa for the plantar heel, 700 kPa for the plantar forefoot, 600 kPa for the plantar toe, and 200 kPa for the rest)	950 kg/m^3	0.4	45,008	Cheung and Zhang, 2005; Ledoux and Blevins, 2007
Profundal fascia	linear triangular shell (S3R)	linearly elastic (Young's modulus: 190 MPa) Thickness: 0.2 mm	950 kg/m^3	0.4	3,971	Hurschler et al., 1994
Bone	linear tetrahedral solid (C3D4)	linearly elastic (Young's modulus: 17,000 MPa)	1990 kg/m^3	0.3	18,965	Bayraktar et al., 2004
Extrinsic foot muscles	Slip ring connector	linearly elastic (stiffness: 157.4 N/mm)	1000 kg/m^3	N/A	N/A	Cook and McDonagh, 1996
Intrinsic foot muscles	Two-node truss (T3D2)	linearly elastic (Young's modulus: 264.8 MPa) Cross-section area: 10 mm^2	1000 kg/m^3	0.4	24	Wong et al., 2016
Rearfoot ligaments	Two-node truss (T3D2)	linearly elastic (Young's modulus: 100–320 MPa) Cross-section area: 7.1–256 mm^2	1000 kg/m^3	0.4	20	Davis et al., 1996; Kura et al., 2001; Milz et al., 1998; Siegler et al., 1988
Other ligaments	Two-node truss (T3D2)	linearly elastic (Young's modulus: 264.8 MPa) Cross-section area: 10 mm^2	1000 kg/m^3	0.4	67	Wong et al., 2016
Plantar fascia	Slip ring connector	linearly elastic (stiffness: 182.4–232.5 N/mm)	1000 kg/m^3	N/A	N/A	Kitaoka et al., 1994
Ground plate	linear tetrahedral solid (C3D4)	linearly elastic (Young's modulus: 17,000 MPa)	1000 kg/m^3	0.3	12,800	N/A

SPH: smoothed-particle hydrodynamics.

plantar connective tissues between RFS and FFS. We hypothesized that FFS would produce a higher foot arch drop, larger plantar ligament stress and plantar fascia tensile force than RFS.

2. Methods

2.1. General information

A habitual rearfoot striker (healthy male aged 29, 170 cm tall, and 65 kg in mass) with twelve-year running experiences, was recruited for the study. The participant reported no musculoskeletal disorders/injuries or orthopedic surgery history prior to the experiment. He was fully informed of the research procedure and signed the consent form. The study was approved by the institution authority (Reference Number: HSEARS20170626003).

2.2. Equipment

A motion capture system with eight optical-based cameras (Vicon, Oxford Metrics Ltd., Oxford, UK) and four force platforms (AMTI, Watertown, USA) were used to collect kinematic and kinetic data. The sampling rates were 250 Hz and 1000 Hz respectively. The maker set was configured to compile with the OpenSim full-body model (Rajagopal et al., 2016). Briefly, markers were affixed to the acromioclavicular joints, lateral/medial humeral epicondyles, radius/ulna styloid processes, posterior/anterior iliac spines, lateral/medial femoral epicondyles, lateral/medial malleoli, calcaneal tuberosity and the base/head of the first and fifth metatarsals.

2.3. Experimental procedure

The participant was asked to run barefoot through the motion capture volume, at the speed of 10 km/h with RFS and FFS, respectively. His running speed was monitored by pairs of photoelectric cells placed along the runway (Hamill et al., 2014). During FFS, the participant was instructed to land with the plantar ball area and lift the heel slightly above the ground. His foot strike pattern was visually observed on-site and further confirmed by the foot strike index (Chen et al., 2016). For each condition, the running trial was repeated ten times and the data of one representative trial were selected for the input of subsequent computational simulation.

Table 2
General gait parameters and initial segmental kinematics.

		RFS	FFS
Measured running speed (m/s)		10.08	10.16
Duration of stance phase (s)		0.27	0.24
Cadence (steps/minute)		168	176
Foot strike index (%)		21.30	69.11
Peak vertical ground reaction force (BW)		2.30	2.44
Averaged loading rate (BW)		52.99	28.90
Initial foot velocity	Anteroposterior (m/s)	2.47 (forward)	2.53 (forward)
	Superoinferior (m/s)	0.54 (downward)	0.70 (downward)
	Mediolateral (m/s)	0.04 (inward)	0.06 (inward)
Initial tibial orientation	Sagittal (degrees)	8.13 (supination)	4.62 (supination)
	Frontal (degrees)	5.01 (inversion)	6.53 (inversion)
	Transversal (degrees)	4.21 (external)	−0.05 (external)
Initial ankle plantarflexion (degrees)		−0.67	18.34

2.4. Musculoskeletal model

The musculoskeletal model (OpenSim, version 3.3, National Center for Simulation in Rehabilitation Research, Stanford, USA) was driven by the kinematic and kinetic data of the selected running trials. The generic model (Rajagopal et al., 2016), featuring 22 rigid-body segments, 37 degrees of freedom and 80 musculotendonous units, was firstly scaled to accommodate the participant's anthropometry. Inverse kinematics was then solved and the dynamic inconsistency was reduced by fine adjustments to the model mass properties (Arnold et al., 2010). Muscle forces were estimated by the Computed Muscle Control module (Thelen, 2003). Joint reaction force and segmental kinematics were generated by the Analyse toolkit and output as the boundary/loading conditions for the FE simulation.

2.5. FE model

2.5.1. Geometry acquisition and reconstruction

MRIs were obtained from the participant's left leg which was fixed at the neutral position using a customized ankle-foot-orthosis (Wong et al., 2014). The 3.0T MRI scanner (GoldSeal Certified Signa HDxt, General Electric Company, Boston, USA) was configurated at T1 sequence, 1-mm slice interval, and a resolution of 0.625 mm pixel size. The images were processed by Mimics and 3-matics (version 19, Materialise, Leuven, Belgium). The geometries of the bulk soft tissue and twenty bony parts, including the distal portion of tibia and fibula, were reconstructed. The bulk soft tissue was encapsulated by a shell unit that encompassed the profundal fascia (internal layer) and skin (external layer) (Fig. 1). The second to fifth interphalangeal joints were fused for simplification. The extrinsic foot muscles and plantar fascia were constructed by slipring connectors while the intrinsic foot muscles and ligaments were constructed by trusses. Their constructions were referenced to the clinic images and were confirmed by an orthopedic surgeon. The material and mesh properties of all components are listed in Table 1. The material of the skin was assigned hyperelastic, while that of the bones, ligaments and muscles were assumed linearly elastic. By reproducing a heel-lift condition (Sharkey et al., 1995), a mesh convergence test was conducted by repeating the simulation with mesh size refinement at 10% interval (from 5.9 mm to 3.2 mm). The overall mesh size was determined to be 3.5 mm such

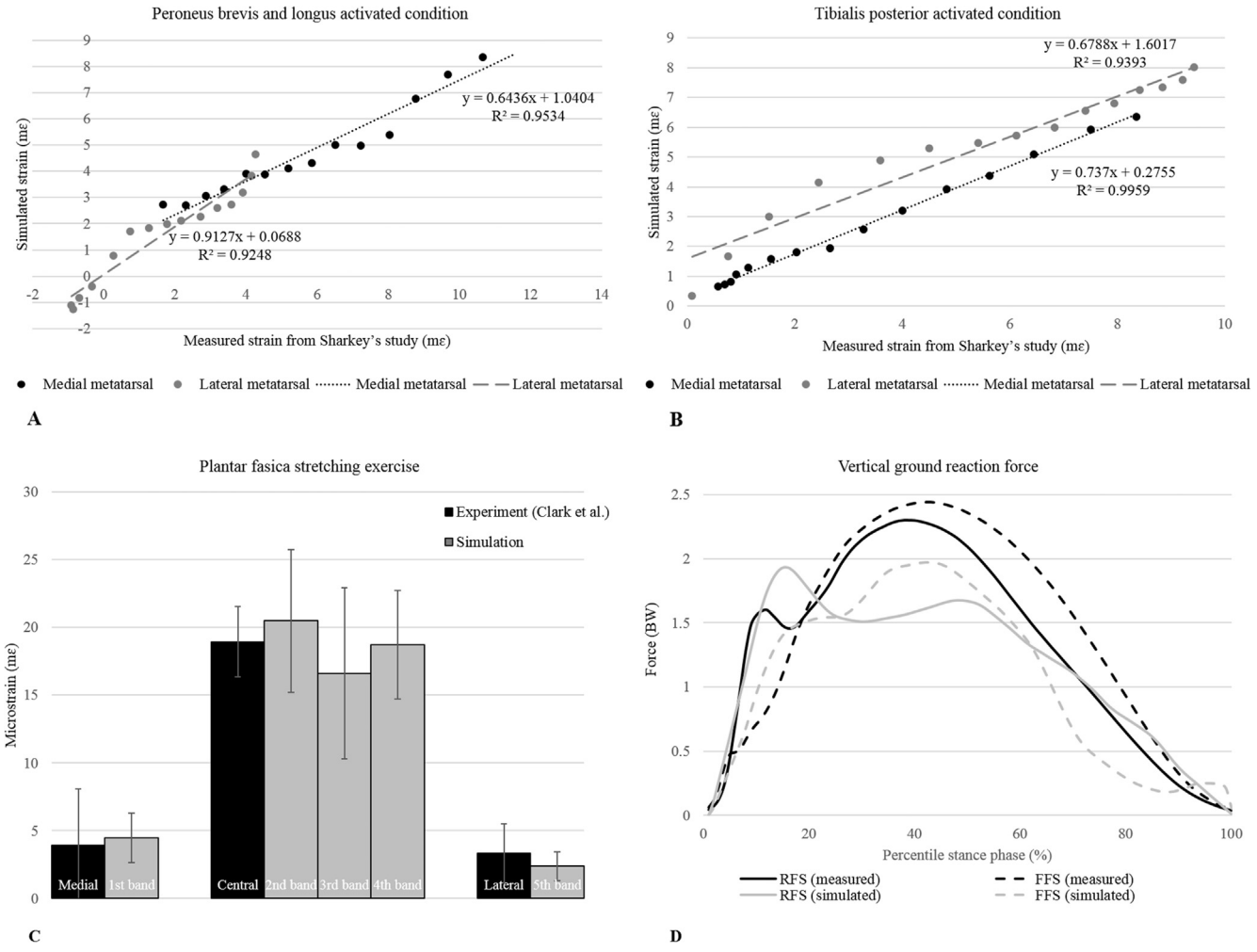

Fig. 2. Validation of the FE foot model by comparing the predicted strain with existing literatures and by comparing the vertical ground reaction force with experimental measurement. (A, B) Linear regression of the second metatarsal bone strain between FE prediction and existing cadaveric study (Sharkey et al., 1995) under a heel-lift condition with (A) peroneus brevis/longus activated or (B) tibialis posterior activated. Each dot denotes the measured and simulated strain value of one measurement point as depicted in Sharkey's study. Parameters of the four trendlines (R2: 0.93–0.99, slope: 0.64–0.91, intercept: 0.276–1.602) indicate a good agreement between the experimental outcomes and model estimation; (C) Comparison of plantar fascia strain between our FE predictions and Clark's study (Clark et al., 2009) in the foot stretching condition. The differences between the measured and simulated strain value were approximately 8.24%–12.33% and did not reach statistical significance ($p < 0.05$) in the independent student t-test; (D) Vertical ground reaction force of RFS and FFS between our FE prediction and experimental measurement. The experimental and simulated GRF in this study were highly correlated for both RFS ($r = 0.921$, $p < 0.01$) and FFS ($r = 0.915$, $p < 0.01$) conditions. RFS: rearfoot strike, FFS: forefoot strike.

that the prediction outcome had less than 5% deviation compared to the last pre-refinement (Henninger et al., 2010). The details were included in the supporting data.

2.5.2. Boundary and loading conditions

The foot model was firstly positioned and orientated with a pre-set ankle joint angulation (Table 2), while the ground plate was fully fixed. The ankle angle was set in a short analytical step at the beginning of the simulation by adjusting the angle between the tibial axial line and the foot longitudinal axis on the sagittal plane. The global coordinate system was configurated based on the OpenSim definition (Delp et al., 2007) to ensure the reference frame was consistent. The initial striking velocity that corresponded to the instant before initial contact was assigned to the foot model. Extrinsic foot muscle force and three-dimensional ankle joint reaction force were applied on the slipring connectors and the tibiotalar articular surface of the talus respectively (Fig. 1). All force data were input in a tabulated time-series matrix sourced from the musculoskeletal model. Gravity was enabled using a force-to-mass ratio of 9.8.

The bone-to-bone interaction was assumed frictionless with non-linear contact to replicate the function of cartilage (Athanasiou et al., 1998). The coefficient of friction between the skin and the ground plate was 0.6 (Zhang and Mak, 1999). The pro-

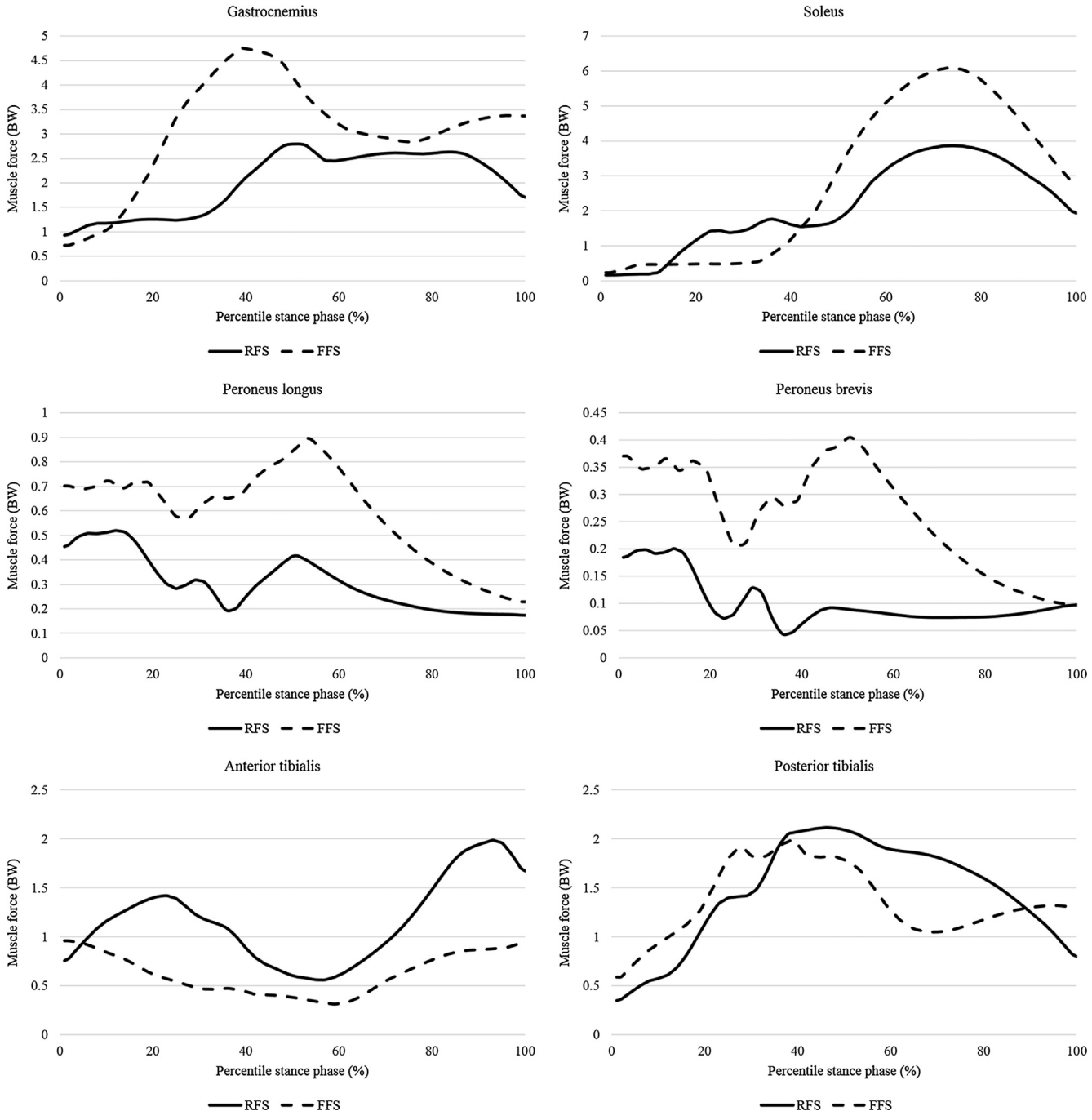

Fig. 3. Extrinsic foot muscle force estimated by the musculoskeletal model. The force is normalized to the bodyweight and scaled to percentile stance phase for both groups. RFS: rearfoot strike, FFS: forefoot strike. RFS: rearfoot strike, FFS: forefoot strike.

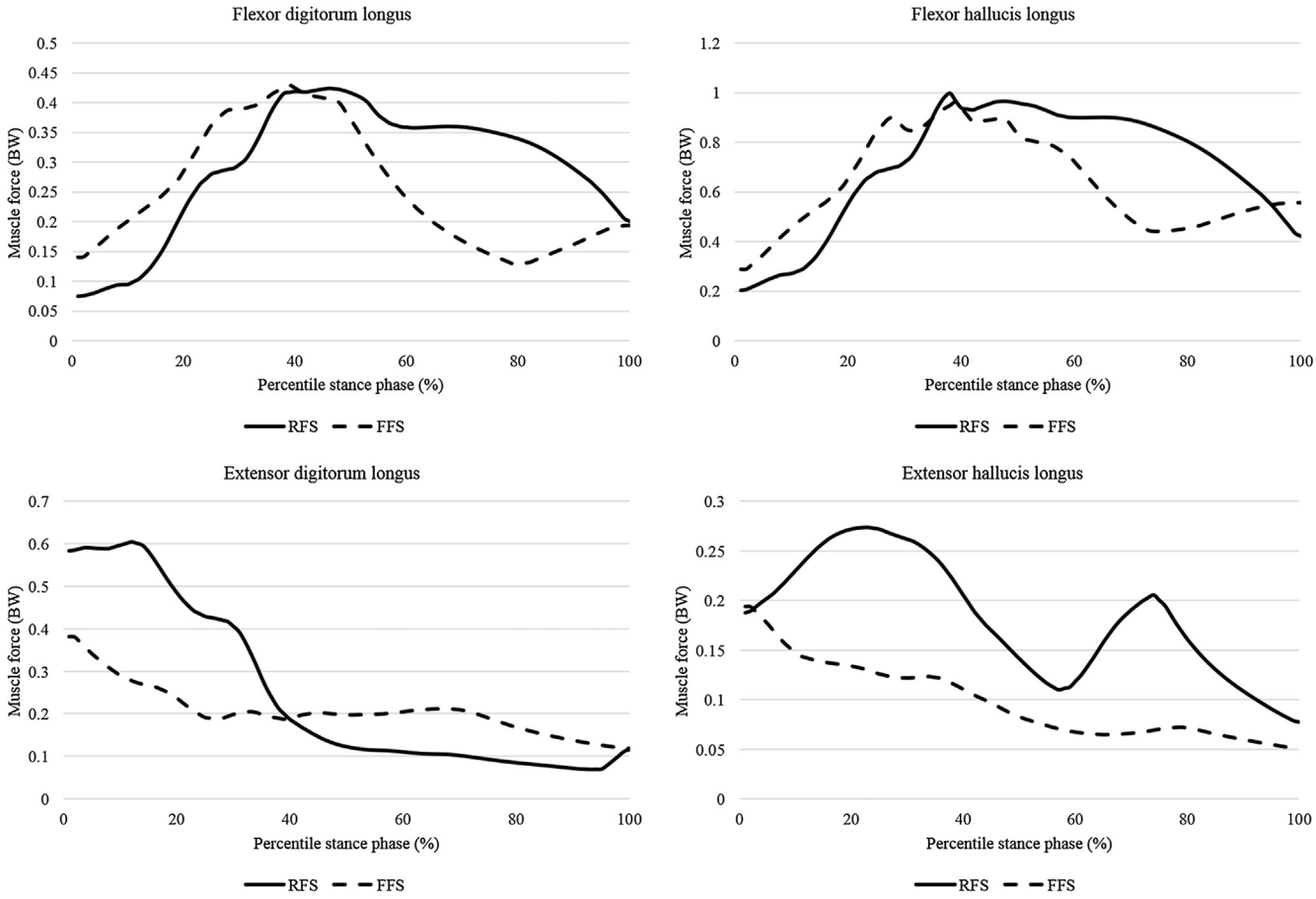

Fig. 3 (*continued*)

fundal fascia surface was tied to the bony surface. The bulk soft tissue was attached to the shell unit using the default cohesive contact property (Fig. 1).

2.5.3. Simulation solver and data output

The simulation was conducted in Abaqus (version 6.14, Dassault Systèmes, Waltham, USA) using the dynamic explicit solver. The foot-ground angle, ankle and first metatarsophalangeal (MTP) joint angle, foot arch deformation, maximum principal stress on the major plantar connective tissues, and the plantar fascia tensile force were reported. The foot-ground angle was defined as the angle between the foot longitudinal axis and the ground surface (positive angle when the foot was upward-tilted). Foot arch deformation was represented by the arch height index (AHI) and medial longitudinal arch (MLA) angle. AHI was the ratio of medial foot arch height at 50% foot length to the truncated foot length (Miller et al., 2014). MLA angle was defined as the angle between the vectors pointing from the navicular tubercle to the first metatarsal head and posterior calcaneus (Prachgosin et al., 2015). Plantar fascia tensile force was the connector force acting on the five fascia bands.

2.5.4. Model validation

Model validation was conducted by reproducing two loading conditions of a cadaveric study (Sharkey et al., 1995). Briefly, the foot was gradually heel-lifted by Achilles/flexor digitorum forces against the ground until the GRF reached 750 N. Meanwhile, either the peroneus brevis/longus or tibialis posterior was loaded by 200 N, depending on the condition simulated. The predicted and measured strain of the second metatarsal was compared using linear regression. The regression parameters (slope, intercept, and R^2) were calculated to demonstrate the accuracy of the FE model. Another set of comparison was conducted by fixing the proximal tibia and loaded the plantar forefoot by 98.1 N (Clark et al., 2009), which imitated a plantar fascia stretching exercise. Strains on the five plantar fascia bands were compared to those reported using an independent student t-test (Clark et al., 2009). We also validated the model by comparing the vertical GRF between the simulation and the measurement by force plates conducted in our study. Pearson correlation (r) and root mean squared error (RMSE) were used to quantify the degree of agreement. All statistics were performed in SPSS (Version 19.0, IBM, Armonk, USA) at a significance level of 0.05.

3. Results

3.1. Model validation

Fig. 2 shows the regression analysis between the predicted and measured second metatarsal strain under the heel-lift condition (Sharkey et al., 1995) with peroneus brevis/longus activated (Fig. 2A) and tibialis posterior activated (Fig. 2B). The Pearson correlation coefficients were between 0.92 and 0.99 (slope: 0.64–0.91, intercept: 0.276–1.602), indicating a good agreement. Fig. 2(C) shows that there was no significant difference between our FE simulation and Clark's study in the plantar fascia strain ($p > 0.05$). Fig. 2(D) demonstrates high correlations between the experimental and simulated GRF for both RFS ($r = 0.921$, $p < 0.01$) and FFS ($r = 0.915$, $p < 0.01$). The RMSE for RFS and FFS was less than one-

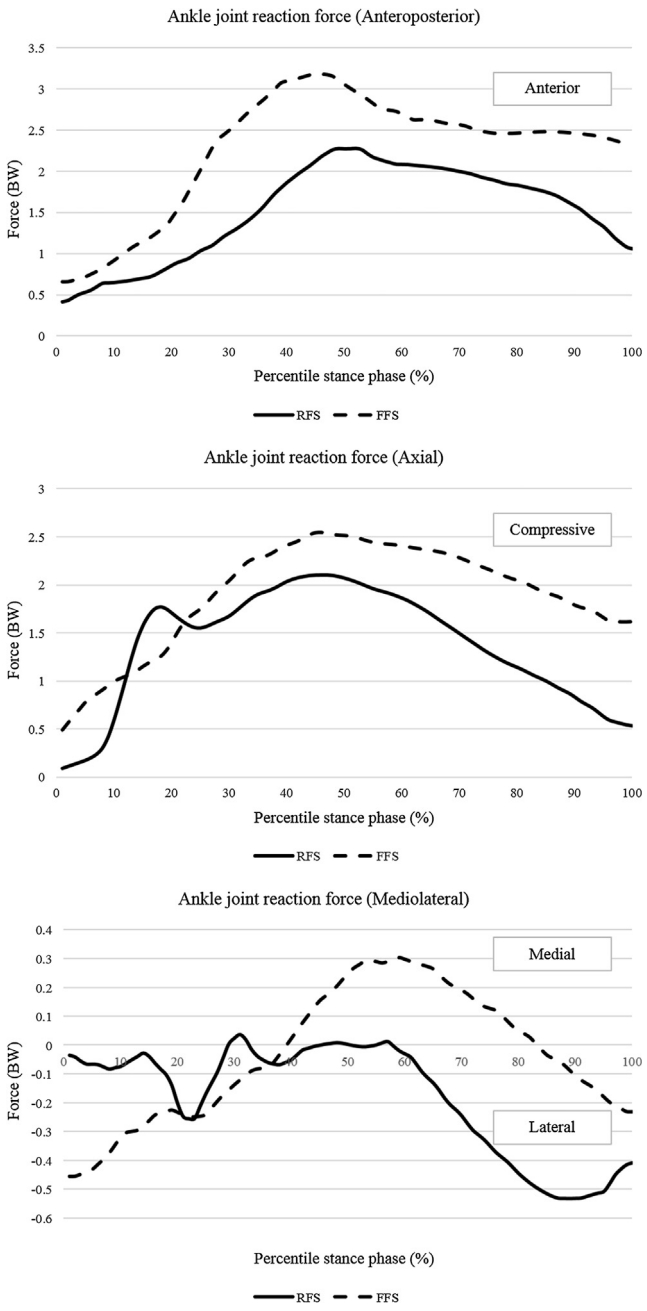

Fig. 4. Ankle joint reaction force estimated by the musculoskeletal model. The force is normalized to the bodyweight and scaled to percentile stance phase for both groups. Positive values mean the force applied in the anterior, inferior, and medial directions with respects to the tibiotalar articular surface of the talus. RFS: rearfoot strike, FFS: forefoot strike.

third bodyweight (BW) which could be attributed to the smaller foot mass resulted from model simplification.

3.2. Spatiotemporal parameters

The running speed was controlled within 5% variance of the target value (Table 2). Foot strike index of each condition fell in the corresponding rearfoot (<33.3%) and forefoot (>66.6%) categories. The participant decreased 11.1% of stance phase duration and increased 4.76% cadence in the transition from RFS to FFS. The peak vertical GRF was comparable between conditions, while FFS reduced the averaged loading rate of vertical GRF by 45.46%.

3.3. Boundary conditions from musculoskeletal model

The two conditions showed apparent differences in muscle force during early- and mid-stance (Fig. 3). Ankle plantarflexors were more activated (57.90–100.49% higher) in FFS, while some ankle dorsiflexors outputs were reduced (29.10–51.73% lower). Peak ankle joint reaction force in FFS was 39.68% (3.19 BW) larger in the anteroposterior direction and 22.98% (2.61 BW) larger in the axial direction (Fig. 4). FFS also produced higher initial foot strike velocity, tibia internally rotation, tibia supination, and ankle plantarflexion during initial contact (Table 2).

3.4. Segmental and joint kinematics from FE simulation

Fig. 5 demonstrated the simulation outcome of running dynamics in our study. As shown in Fig. 6(A–C), The most prominent kinematic differences occurred at initial contact. In FFS, the participant reduced the foot-ground angle (down-tilt the foot) by 22.61° and increased ankle plantarflexion by 19.01°. Meanwhile, the peak first MTP joint dorsiflexion in FFS was 15.44° higher compared to RFS.

Fig. 6(E) and (D) show that FFS generated a notable drop in foot arch height shortly after the initial contact. The minimal AHI was 9.12% lower in FFS (0.24) compared to RFS (0.27). Correspondingly, MLA angle increased rapidly in FFS during the first half of the stance phase and reached its peak of 137.66° at mid-stance, which was 2.06% higher than that of RFS (134.73°).

3.5. Plantar connective tissue loading from FE simulation

All examined connective tissues were apparently more loaded in FFS (Fig. 7), except for the flexor hallucis brevis. The peak principal maximal stress was about one-fifth to two-fold higher in FFS. The plantar ligaments shared a greater proportion of the increased foot arch loading in FFS. Stress increments in plantar ligaments (0.93–9.67 MPa) were higher than that of the intrinsic foot muscles (0.35–0.37 MPa). Tensile force of the plantar fascia was generally higher in FFS for the first to fourth bands (Fig. 8), in which the maximal force could be 18.71–109.10% higher.

4. Discussion

The main purpose of this study was to explore the biomechanical behavior of the foot arch and plantar connective tissues in running with different foot strike techniques. The significance of this study resided in its potentials to reveal the risks of plantar fasciitis inherent in foot strike pattern modification. Our findings supported the hypothesis that FFS increased the foot arch deformation, plantar connective tissue stress, and tensile force on the plantar fascia.

We adopted an smoothed-particle hydrodynamics (SPH) method in modeling the bulk soft tissue. SPH presented several advantages because it avoided extreme mesh distortions that were frequently encountered in highly impact problems (Johnson et al., 1996). The SPH implemented a cohesive contact property with the boundary FE mesh and could accommodate high deformation and propagation speed (Fig. 5). The interval distance between the SPH particles was 1–1.5 mm in our study, which was believed to be sufficiently fine (Jankowiak and Łodygowski, 2013). Previous studies reported that SPH provided accurate results in simulating impact (Kulper et al., 2018) and was now applied to running dynamics.

Our results were similar to that of previous literature. Existing studies reported that the alterations of foot and joint angle between RFS and FFS mostly occurred at initial contact. Depending on research setups, the foot-ground angle at landing could range from 7.60° to 14.85° for RFS and from −12.46° to −3.37° for FFS (Nunns et al., 2013; Shih et al., 2013; Williams et al., 2000,

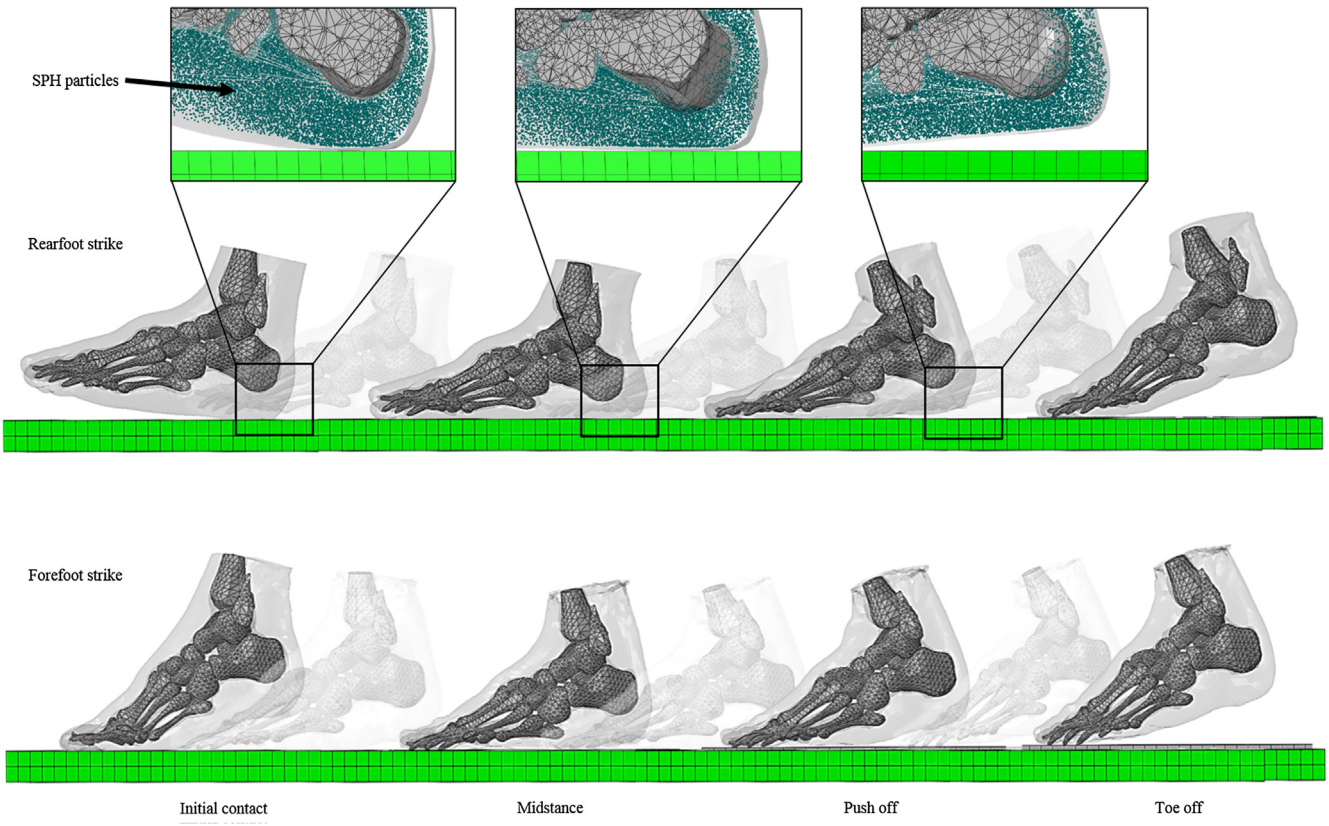

Fig. 5. Dynamic simulation of RFS and FFS running. The movement of the FE foot model was continuous from the initial contact to toe-off phase. The SPH particles representing the soft tissue were compressed and attached to the shell unit (the profundal fascia and skin) during impact. SPH: smoothed-particle hydrodynamics.

2012). Ankle angle at landing ranged from 10.08° to 24.80° for RFS and from −12.46° to 2.3° for FFS (Kulmala et al., 2013; Shih et al., 2013; Williams et al., 2012). MTP joint motion was rarely observed, but it was reasonable for the runner to dorsiflex his toe in FFS as a mean to increase the contact area of the forefoot. Landing with down-tilt foot/plantarflexed ankle in FFS facilitated a larger ankle joint excursion and negative work done by the calf muscles to resist heel drop and to absorb impact.

Previous studies measuring EMG signals also found that FFS increased ankle plantarflexor (5.10–23.53% higher in Achilles tendon tension) and decreased ankle dorsiflexor activities (54.48–75.00% lower in anterior tibialis) (Kulmala et al., 2013; Landreneau et al., 2014; Rice and Patel, 2017; Yong et al., 2014). The increased ankle joint motion and calf muscle force in FFS were considered as the primary contributor to the reduced loading rate of the vertical GRF (Kulmala et al., 2013; Shih et al., 2013), and the trend of increased ankle joint loading (Rooney and Derrick, 2013). All these factors could influence the bending force on the foot arch and cause excessive arch deformation.

Excessive arch deformation was associated with plantar tissues overload and the pathologies of ligamentous injuries (Tao et al., 2010; Thordarson et al., 1995). The changes of AHI reported by our simulation was in accordance with previous studies (0.028 in running) (Hageman, 2010). MLA angular changes were also found similar to the value measured by fluoroscopy (2.3–6.1°) (Fukano and Fukubayashi, 2012). Under the non-weight bearing condition, the increased Achilles tension and MTP dorsiflexion should have elevated the foot arch due to the tightening of the plantar connective tissues (Bolgla and Malone, 2004). Instead, the plantar connective tissues underwent elongation as a result of compression from the arch top in FFS running (Morales-Orcajo et al., 2018).

Plantar connective tissues are important components of the multi-layer load-bearing system of the foot arch (Kirby, 2017). The present study demonstrated the synergy among foot muscles, plantar ligaments and plantar fascia (Crary et al., 2003). Research reported that the range of plantar fascia tension was 464–922 N during walking (Chen et al., 2014; Erdemir et al., 2004; Lin et al., 2014), which was relatively high compared to our study (372 N in RFS). One possible explanation could be that the disregard of some muscle forces could transfer the total foot arch load to other arch stabilizers (Kirby, 2017). Our predicted increases of plantar fascia force in FFS (18.71%−109.10%) were also larger than that (9.57%) of McDonald's (McDonald et al., 2016) because the influence of foot arch deformation was considered in the present study. Our findings were supported by another FE study (Li et al., 2017), which reported a higher stress level and stress increase rate on the metatarsal bones in FFS than RFS. A larger external force applied to the plantar forefoot in FFS could further stretch the plantar fascia due to the bending strain to the whole foot (Kernozek et al., 2014, 2016).

The fatigue life of the fascia tissue was mainly determined by the maximal stress range that it sustained in the loading cycles (Carter et al., 1981). Therefore, the increased peak fascia tension in FFS was likely to reduce the sustainable gait cycles before localized damage occurred. Additionally, habitual RFS runners usually increased their cadence when running in FFS at the same speed (Baggaley et al., 2017). The increased loading in each cycle, together with the higher step frequency, would expose the runner to a faster pathological process if the same running regime of RFS is carried over to FFS. This could be the reason that mainstream gait retraining programs emphasize the importance of a step-by-step procedure for runners to adopt FFS (Huffer et al., 2017). They suggested to reduce running volume and strengthen foot muscle at the

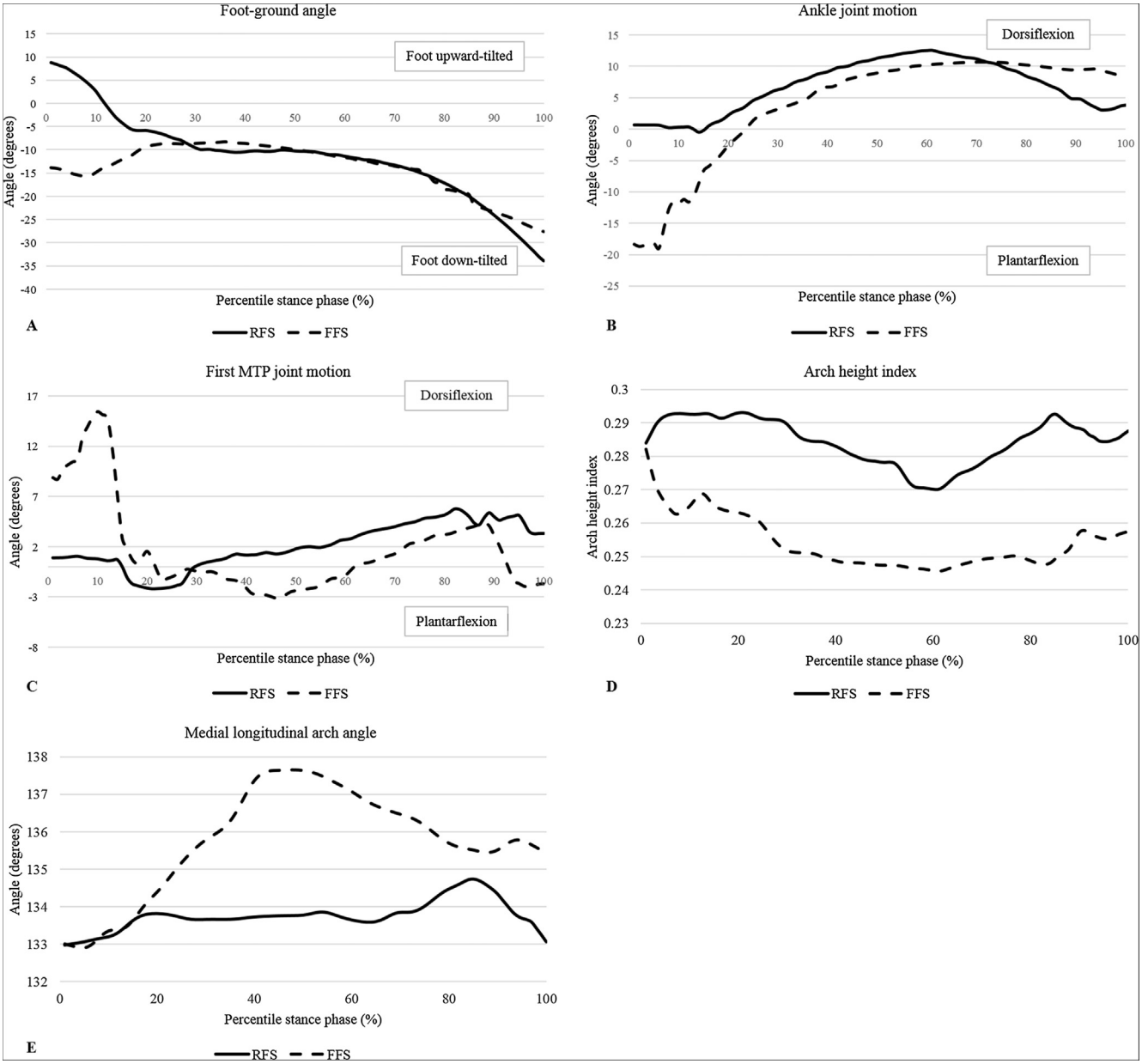

Fig. 6. Segmental kinematics predicted by the FE analysis: (A) foot-ground angle; (B) Ankle joint motion; (C) First MTP joint motion; (D) Arch height index; (E) Medial longitudinal arch angle. All variables are scaled to percentile stance phase for both groups. Foot-ground angle is the angle between the foot longitudinal axis and the ground surface. The ankle and MTP joints are dorsiflexed/plantarflexed on the sagittal plane. Positive values mean that the foot is upward-tilted with respects to the ground and the ankle/MTP joint is dorsiflexed. MTP: metatarsophalangeal, RFS: rearfoot strike, FFS: forefoot strike.

early training stage, to avoid plantar fascia overload (Cheung et al., 2015). As a mean to minimize the incidence of plantar fasciitis, runners should adjust their gait patterns with cares and also follow the professional guidance.

Besides the simplification and assumption made in the modeling procedure, the single-subject design was the major limitation of our study. The problem was commonly faced by research using a theoretical approach, e.g., finite element method. The material of the ligaments and muscles were assumed linearly elastic despite that they exhibit hyperelastic or viscoelastic behavior. The approach may underestimate the joint stiffness of the model, while it remains a common simplification strategy in FE foot model to compromise computational efficiency, in addition to the fact that the material property profile of some foot ligaments is incomplete (Morales-Orcajo et al., 2016). As foot strike patterns influenced muscle activities, measuring EMG signals of the leg muscles could enrich the inputs to the simulation and increase the accuracy of force prediction. The healthy participant recruited was assumed to represent the typical characteristics of the runner population. However, individual variances in foot geometries, gait characteristics, and running regime were not considered. A prospective study tracking the injury progression for both RFS and FFS runners would provide more insight into the foot problem.

Acknowledgements

The study was financially supported by: Key R&D Program granted by the Ministry of Science and Technology of China (No.: 2018YFB1107000), General Research Fund granted by the Hong Kong Research Grant Council (No.: PolyU152065/17E), NFSC granted by the National Natural Science Foundation of China (No.: 11732015), and Shenzhen Research Fund granted by the

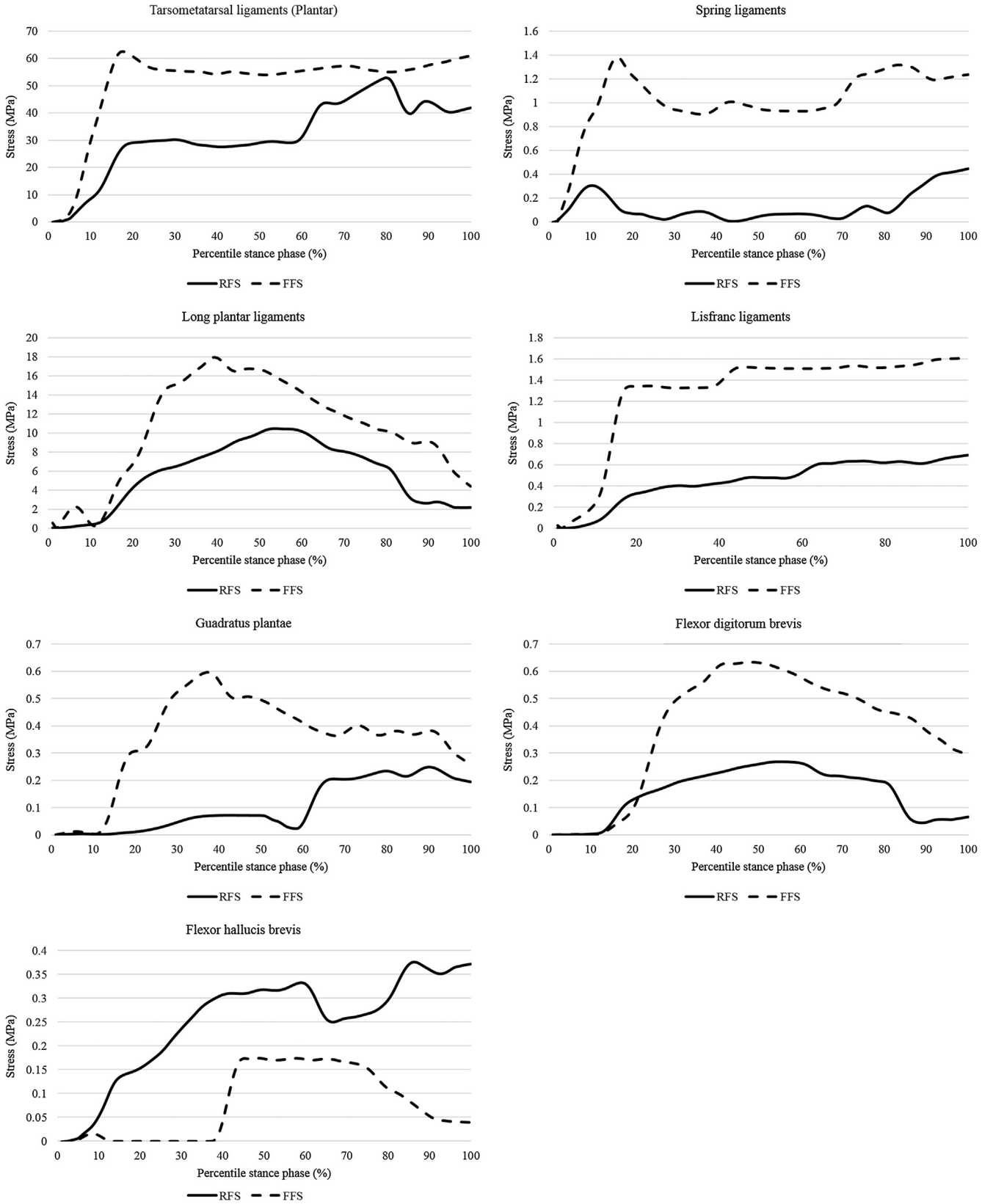

Fig. 7. Principal maximal stress on the major plantar foot ligaments and intrinsic foot muscles. All variables are scaled to percentile stance phase for both groups. RFS: rearfoot strike, FFS: forefoot strike.

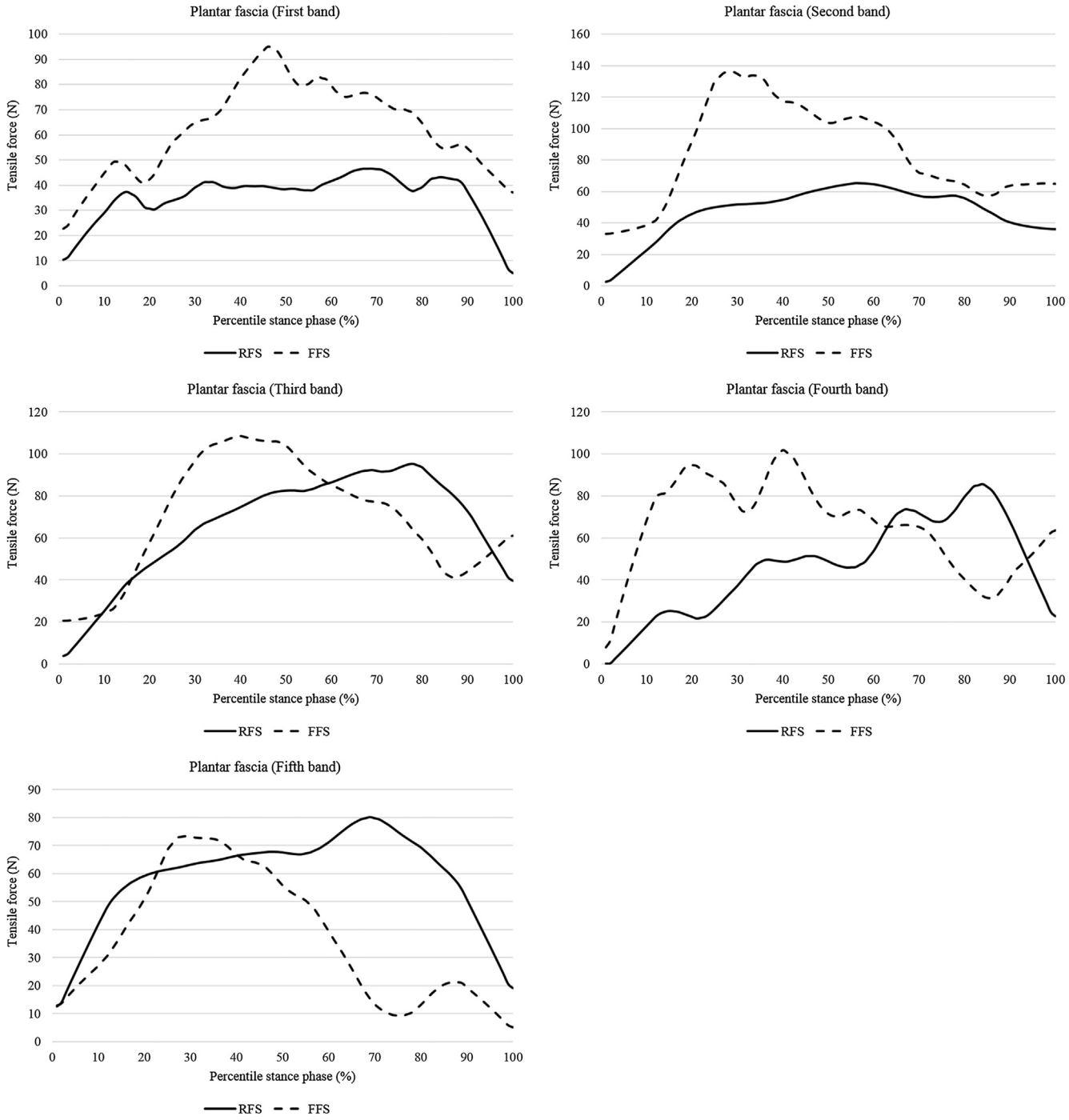

Fig. 8. Tensile force on the five plantar fascia bands. All variables are scaled to percentile stance phase for both groups. RFS: rearfoot strike, FFS: forefoot strike.

Shenzhen Science and Technology Innovation Committee (No.: JCYJ-20160531-18462-1718).

Conflict of interest statement

The authors do not have any financial and personal relationships with other people or organizations that inappropriately influence the work performed.

Appendix A. Supplementary material

Supplementary data to this article can be found online at https://doi.org/10.1016/j.jbiomech.2018.12.007.

References

Almeida, M.O., Davis, I.S., Lopes, A.D., 2015. Biomechanical differences of foot-strike patterns during running: a systematic review with meta-analysis. J. Orthop. Sports Phys. Ther. 45, 738–755. https://doi.org/10.2519/jospt.2015.6019.

Altman, A.R., Davis, I.S., 2012. A kinematic method for footstrike pattern detection in barefoot and shod runners. Gait Posture 35, 298–300. https://doi.org/10.1016/j.gaitpost.2011.09.104.

Arnold, E.M., Ward, S.R., Lieber, R.L., Delp, S.L., 2010. A model of the lower limb for analysis of human movement. Ann. Biomed. Eng. 38, 269–279. https://doi.org/10.1007/s10439-009-9852-5.

Athanasiou, K.A., Liu, G.T., Lavery, L.A., Lanctot, D.R., Schenck, R.C., 1998. Biomechanical topography of human articular cartilage in the first metatarsophalangeal joint. Clin. Orthop. Relat. Res., 269–281

Baggaley, M., Willy, R.W., Meardon, S.A., 2017. Primary and secondary effects of real-time feedback to reduce vertical loading rate during running. Scand. J. Med. Sci. Sports 27, 501–507. https://doi.org/10.1111/sms.12670.

Bayraktar, H.H., Morgan, E.F., Niebur, G.L., Morris, G.E., Wong, E.K., Keaveny, T.M., 2004. Comparison of the elastic and yield properties of human femoral trabecular and cortical bone tissue. J. Biomech. 37, 27–35. https://doi.org/10.1016/S0021-9290(03)00257-4.

Behforootan, S., Chatzistergos, P., Naemi, R., Chockalingam, N., 2017. Finite element modelling of the foot for clinical application: a systematic review. Med. Eng. Phys. 39, 1–11. https://doi.org/10.1016/j.medengphy.2016.10.011.

Bruening, D.A., Cooney, K.M., Buczek, F.L., 2012. Analysis of a kinetic multi-segment foot model part II: kinetics and clinical implications. Gait Posture 35, 535–540. https://doi.org/10.1016/j.gaitpost.2011.11.012.

Carter, D.R., Caler, W.E., Spengler, D.M., Frankel, V.H., 1981. Fatigue behavior of adult cortical bone: the influence of mean strain and strain range. Acta Orthopaed. 52, 481–490.

Chen, T., An, W., Chan, Z., Au, I., Zhang, Z., Cheung, R., 2016. Immediate effects of modified landing pattern on a probabilistic tibial stress fracture model in runners. Clin. Biomech. 33, 49–54. https://doi.org/10.1016/j.clinbiomech.2016.02.013.

Chen, W.-M., Lee, P.V.-S., 2015. Explicit finite element modelling of heel pad mechanics in running: inclusion of body dynamics and application of physiological impact loads. Comp. Meth. Biomech. Biomed. Eng. 18, 1582–1595. https://doi.org/10.1080/10255842.2014.930447.

Chen, Y.-N., Chang, C.-W., Li, C.-T., Chang, C.-H., Lin, C.-F., 2014. Finite element analysis of plantar fascia during walking: a quasi-static simulation. Foot Ankle Int. 1071100714549189.

Cheung, J.T.-M., Zhang, M., 2005. A 3-dimensional finite element model of the human foot and ankle for insole design. Arch. Phys. Med. Rehab. 86, 353–358. https://doi.org/10.1016/j.apmr.2004.03.031.

Cheung, R.T.H., Sze, L.K.Y., Mok, N.W., Ng, G.Y.F., 2015. Intrinsic foot muscle volume in experienced runners with and without chronic plantar fasciitis. J. Sci. Med. Sport. https://doi.org/10.1016/j.jsams.2015.11.004.

Clark, R.A., Franklyn-Miller, A., Falvey, E., Bryant, A.L., Bartold, S., McCrory, P., 2009. Assessment of mechanical strain in the intact plantar fascia. The Foot 19, 161–164. https://doi.org/10.1016/j.foot.2009.06.001.

Cook, C.S., McDonagh, M.J.N., 1996. Measurement of muscle and tendon stiffness in man. Eur. J. Appl. Physiol. Occup. Physiol. 72, 380–382. https://doi.org/10.1007/BF00599700.

Crary, J.L., Hollis, J.M., Manoli, A., 2003. The effect of plantar fascia release on strain in the spring and long plantar ligaments. Foot Ankle Int. 24, 245–250.

Daoud, A.I., Geissler, G.J., Wang, F., Saretsky, J., Daoud, Y.A., Lieberman, D.E., 2012. Foot strike and injury rates in endurance runners: a retrospective study. Med. Sci. Sports Exerc. 44, 1325–1334. https://doi.org/10.1249/MSS.0b013e3182465115.

Davis, W.H., Sobel, M., DiCarlo, E.F., Torzilli, P.A., Deng, X., Geppert, M.J., Patel, M.B., Deland, J., 1996. Gross, histological, and microvascular anatomy and biomechanical testing of the spring ligament complex. Foot Ankle Int. 17, 95–102.

Delp, S.L., Anderson, F.C., Arnold, A.S., Loan, P., Habib, A., John, C.T., Guendelman, E., Thelen, D.G., 2007. OpenSim: open-source software to create and analyze dynamic simulations of movement. IEEE Trans. Biomed. Eng. 54, 1940–1950. https://doi.org/10.1109/TBME.2007.901024.

Erdemir, A., Hamel, A.J., Fauth, A.R., Piazza, S.J., Sharkey, N.A., 2004. Dynamic loading of the plantar aponeurosis in walking. J. Bone Joint Surg. Am. 86, 546–552.

Fukano, M., Fukubayashi, T., 2012. Gender-based differences in the functional deformation of the foot longitudinal arch. The Foot 22, 6–9. https://doi.org/10.1016/j.foot.2011.08.002.

Hageman, E.R., 2010. Medial longitudinal arch mechanics before and after a prolonged run (Graduate Theses and Dissertations). Iowa State University https://doi.org/10.31274/etd-180810-1788.

Hamill, J., Gruber, A.H., Derrick, T.R., 2014. Lower extremity joint stiffness characteristics during running with different footfall patterns. Eur. J. Sport Sci. 14, 130–136. https://doi.org/10.1080/17461391.2012.728249.

Henninger, H.B., Reese, S.P., Anderson, A.E., Weiss, J.A., 2010. Validation of computational models in biomechanics. Proc. Inst. Mech. Eng., Part H: J. Eng. Med. 224, 801–812.

Huffer, D., Hing, W., Newton, R., Clair, M., 2017. Strength training for plantar fasciitis and the intrinsic foot musculature: a systematic review. Phys. Ther. Sport 24, 44–52. https://doi.org/10.1016/j.ptsp.2016.08.008.

Hurschler, C., Vanderby, R., Martinez, D.A., Vailas, A.C., Turnipseed, W.D., 1994. Mechanical and biochemical analyses of tibial compartment fascia in chronic compartment syndrome. Ann. Biomed. Eng. 22, 272–279.

Jankowiak, T., Łodygowski, T., 2013. Smoothed particle hydrodynamics versus finite element method for blast impact. Bull. Polish Acad. Sci.: Tech. Sci. 61, 111–121. https://doi.org/10.2478/bpasts-2013-0009.

Johnson, G.R., Stryk, R.A., Beissel, S.R., 1996. SPH for high velocity impact computations. Comput. Meth Appl. Mech. Eng. 139, 347–373. https://doi.org/10.1016/S0045-7825(96)01089-4.

Kernozek, T., Meardon, S., Vannatta, C., 2014. In-shoe loading in rearfoot and non-rearfoot strikers during running using minimalist footwear. Int. J. Sports Med. 35, 1112–1117. https://doi.org/10.1055/s-0034-1372627.

Kernozek, T.W., Vannatta, C.N., Gheidi, N., Kraus, S., Aminaka, N., 2016. Plantar loading changes with alterations in foot strike patterns during a single session in habitual rear foot strike female runners. Phys. Therapy Sport 18, 32–37. https://doi.org/10.1016/j.ptsp.2015.05.004.

Kirby, K.A., 2017. Longitudinal arch load-sharing system of the foot. Revista Española de Podología 28, e18–e26. https://doi.org/10.1016/j.repod.2017.03.003.

Kitaoka, H.B., Luo, Z.P., Growney, E.S., Berglund, L.J., An, K.N., 1994. Material properties of the plantar aponeurosis. Foot Ankle Int. 15, 557–560.

Knorz, S., Kluge, F., Gelse, K., Schulz-Drost, S., Hotfiel, T., Lochmann, M., Eskofier, B., Krinner, S., 2017. Three-dimensional biomechanical analysis of rearfoot and forefoot running 2325967117719065 Orthop. J. Sports Med. 5. https://doi.org/10.1177/2325967117719065.

Kulmala, J.-P., Avela, J., Pasanen, K., Parkkari, J., 2013. Forefoot strikers exhibit lower running-induced knee loading than rearfoot strikers. Med. Sci. Sports Exerc. 45, 2306–2313. https://doi.org/10.1249/MSS.0b013e31829efcf7.

Kulper, S.A., Fang, C.X., Ren, X., Guo, M., Sze, K.Y., Leung, F.K.L., Lu, W.W., 2018. Development and initial validation of a novel smoothed-particle hydrodynamics-based simulation model of trabecular bone penetration by metallic implants. J. Orthop. Res. 36, 1114–1123. https://doi.org/10.1002/jor.23734.

Kura, H., Luo, Z.-P., Kitaoka, H.B., Smutz, W.P., An, K.-N., 2001. Mechanical behavior of the Lisfranc and dorsal cuneometatarsal ligaments: in vitro biomechanical study. J. Orthopaed. Trauma 15, 107–110.

Landreneau, L.L., Watts, K., Heitzman, J.E., Childers, W.L., 2014. Lower limb muscle activity during forefoot and rearfoot strike running techniques. Int. J. Sports Phys. Ther. 9, 888–897.

Ledoux, W.R., Blevins, J.J., 2007. The compressive material properties of the plantar soft tissue. J. Biomech. 40, 2975–2981. https://doi.org/10.1016/j.jbiomech.2007.02.009.

Li, S., Zhang, Y., Gu, Y., Ren, J., 2017. Stress distribution of metatarsals during forefoot strike versus rearfoot strike: a finite element study. Comp. Biol. Med. 91, 38–46. https://doi.org/10.1016/j.compbiomed.2017.09.018.

Lieberman, D.E., 2012. What we can learn about running from barefoot running: an evolutionary medical perspective. Exerc. Sport Sci. Rev. 40, 63–72. https://doi.org/10.1097/JES.0b013e31824ab210.

Lieberman, D.E., Venkadesan, M., Werbel, W.A., Daoud, A.I., D'Andrea, S., Davis, I.S., Mang'eni, R.O., Pitsiladis, Y., 2010. Foot strike patterns and collision forces in habitually barefoot versus shod runners. Nature 463, 531–535. https://doi.org/10.1038/nature08723.

Lin, S.-C., Chen, C.P.-C., Tang, S.F.-T., Chen, C.-W., Wang, J.-J., Hsu, C.-C., Hsieh, J.-H., Chen, W.-P., 2014. Stress distribution within the plantar aponeurosis during walking — a dynamic finite element analysis. J. Mech. Med. Biol. 14, 1450053. https://doi.org/10.1142/S0219519414500535.

McDonald, K.A., Stearne, S.M., Alderson, J.A., North, I., Pires, N.J., Rubenson, J., 2016. The role of arch compression and metatarsophalangeal joint dynamics in modulating plantar fascia strain in running. PLoS One 11. https://doi.org/10.1371/journal.pone.0152602.

Miller, E.E., Whitcome, K.K., Lieberman, D.E., Norton, H.L., Dyer, R.E., 2014. The effect of minimal shoes on arch structure and intrinsic foot muscle strength. J. Sport Health Sci. 3, 74–85. https://doi.org/10.1016/j.jshs.2014.03.011.

Milz, P., Milz, S., Steinborn, M., Mittlmeier, T., Putz, R., Reiser, M., 1998. Lateral ankle ligaments and tibiofibular syndesmosis. 13-MHz high-frequency sonography and MRI compared in 20 patients. Acta Orthop. Scand. 69, 51–55. https://doi.org/10.3109/17453679809002357.

Morales-Orcajo, E., Bayod, J., de Las, Barbosa, Casas, E., 2016. Computational foot modeling: scope and applications. Arch. Comput. Meth. Eng. 23, 389–416. https://doi.org/10.1007/s11831-015-9146-z.

Morales-Orcajo, E., de Bengoa, Becerro, Vallejo, R., Losa Iglesias, M., Bayod, J., de Las, Barbosa, Casas, E., 2018. Foot internal stress distribution during impact in barefoot running as function of the strike pattern. Comp. Meth. Biomech. Biomed. Eng. 1–8. https://doi.org/10.1080/10255842.2018.1480760.

Nunns, M., House, C., Fallowfield, J., Allsopp, A., Dixon, S., 2013. Biomechanical characteristics of barefoot footstrike modalities. J. Biomech. 46, 2603–2610. https://doi.org/10.1016/j.jbiomech.2013.08.009.

Pailler-Mattei, C., Bec, S., Zahouani, H., 2008. In vivo measurements of the elastic mechanical properties of human skin by indentation tests. Med. Eng. Phys. 30, 599–606. https://doi.org/10.1016/j.medengphy.2007.06.011.

Paquette, M.R., Zhang, S., Baumgartner, L.D., 2013. Acute effects of barefoot, minimal shoes and running shoes on lower limb mechanics in rear and forefoot strike runners. Footwear Sci. 5, 9–18. https://doi.org/10.1080/19424280.2012.692724.

Perkins, K.P., Hanney, W.J., Rothschild, C.E., 2014. The risks and benefits of running barefoot or in minimalist shoes: a systematic review. Sports Health: Multidisciplinary Approach 6, 475–480. https://doi.org/10.1177/1941738114546846.

Perl, D.P., Daoud, A.I., Lieberman, D.E., 2012. Effects of footwear and strike type on running economy. Med. Sci. Sports Exerc. 44, 1335–1343. https://doi.org/10.1249/MSS.0b013e318247989e.

Prachgosin, T., Chong, D.Y.R., Leelasamran, W., Smithmaitrie, P., Chatpun, S., 2015. Medial longitudinal arch biomechanics evaluation during gait in subjects with flexible flatfoot. Acta Bioeng. Biomech. 10.5277/abb-00296-2015-02.

Rajagopal, A., Dembia, C.L., DeMers, M.S., Delp, D.D., Hicks, J.L., Delp, S.L., 2016. Full-body musculoskeletal model for muscle-driven simulation of human gait. IEEE Trans. Biomed. Eng. 63, 2068–2079. https://doi.org/10.1109/TBME.2016.2586891.

Rice, H., Patel, M., 2017. Manipulation of foot strike and footwear increases Achilles tendon loading during running. Am. J. Sports Med. 45, 2411–2417. https://doi.org/10.1177/0363546517704429.

Rooney, B.D., Derrick, T.R., 2013. Joint contact loading in forefoot and rearfoot strike patterns during running. J. Biomech. 46, 2201–2206. https://doi.org/10.1016/j.jbiomech.2013.06.022.

Roxas, M., 2005. Plantar fasciitis: diagnosis and therapeutic considerations. Altern. Med. Rev. 10, 83–93.
Sharkey, N.A., Ferris, L., Smith, T.S., Matthews, D.K., 1995. Strain and loading of the second metatarsal during heel-lift. J. Bone Joint Surg. Am. 77, 1050–1057.
Shih, Y., Lin, K.-L., Shiang, T.-Y., 2013. Is the foot striking pattern more important than barefoot or shod conditions in running? Gait Posture 38, 490–494. https://doi.org/10.1016/j.gaitpost.2013.01.030.
Siegler, S., Block, J., Schneck, C.D., 1988. The mechanical characteristics of the collateral ligaments of the human ankle joint. Foot Ankle 8, 234–242.
Tao, K., Ji, W.-T., Wang, D.-M., Wang, C.-T., Wang, X., 2010. Relative contributions of plantar fascia and ligaments on the arch static stability: a finite element study. Biomedizinische Technik/Biomed. Eng. 55, 265–271. https://doi.org/10.1515/bmt.2010.041.
Taunton, J.E., Ryan, M.B., Clement, D.B., McKenzie, D.C., Lloyd-Smith, D.R., Zumbo, B. D., 2002. A retrospective case-control analysis of 2002 running injuries. Br. J. Sports Med 36, 95–101.
Thelen, D.G., 2003. Adjustment of muscle mechanics model parameters to simulate dynamic contractions in older adults. J. Biomech. Eng. 125, 70. https://doi.org/10.1115/1.1531112.
Thordarson, D.B., Schmotzer, H., Chon, J., Peters, J., 1995. Dynamic support of the human longitudinal arch: a biomechanical evaluation. Clin. Orthopaed. Related Res. 316, 165–172.
van Gent, R.N., Siem, D., van Middelkoop, M., van Os, A.G., Bierma-Zeinstra, S.M.A., Koes, B.W., 2007. Incidence and determinants of lower extremity running injuries in long distance runners: a systematic review. Br. J. Sports Med. 41, 469–480. https://doi.org/10.1136/bjsm.2006.033548. discussion 480.
Wearing, S.C., Smeathers, J.E., Urry, S.R., Hennig, E.M., Hills, A.P., 2006. The pathomechanics of plantar fasciitis. Sports Med. 36, 585–611.
Williams, D.S., McClay, I.S., Manal, K.T., 2000. Lower extremity mechanics in runners with a converted forefoot strike pattern. J. Appl. Biomech. 16, 210–218. https://doi.org/10.1123/jab.16.2.210.
Williams, D.S.B., Green, D.H., Wurzinger, B., 2012. Changes in lower extremity movement and power absorption during forefoot striking and barefoot running. Int. J. Sports Phys. Ther. 7, 525–532.
Wong, D.W.-C., Niu, W., Wang, Y., Zhang, M., 2016. Finite element analysis of foot and ankle impact injury: risk evaluation of calcaneus and talus fracture. PLoS ONE 11, e0154435. https://doi.org/10.1371/journal.pone.0154435.
Wong, D.W.-C., Zhang, M., Yu, J., Leung, A.K.-L., 2014. Biomechanics of first ray hypermobility: an investigation on joint force during walking using finite element analysis. Med. Eng. Phys. 36, 1388–1393. https://doi.org/10.1016/j.medengphy.2014.03.004.
Yong, J.R., Silder, A., Delp, S.L., 2014. Differences in muscle activity between natural forefoot and rearfoot strikers during running. J. Biomech. 47, 3593–3597. https://doi.org/10.1016/j.jbiomech.2014.10.015.
Zhang, M., Mak, A.F., 1999. In vivo friction properties of human skin. Prosthet Orthot Int. 23, 135–141. https://doi.org/10.3109/03093649909071625.